



Synthesis and characterization of binary transition metal oxide/reduced graphene oxide nanocomposites and its enhanced electrochemical properties for supercapacitor applications

S. Nagarani¹ · G. Sasikala¹ · K. Satheesh² · M. Yuvaraj³ · R. Jayavel¹

Received: 5 February 2018 / Accepted: 10 May 2018 / Published online: 30 May 2018
© Springer Science+Business Media, LLC, part of Springer Nature 2018

Abstract

$\text{SnO}_2/\text{Co}_3\text{O}_4$ (BTMO) with reduced graphene oxide (rGO) nanocomposite were synthesized by co-precipitation method to determine its electrochemical properties for the betterment of Supercapacitor applications. The XRD pattern of BTMO/rGO nanocomposite shows tetragonal rutile and spinal cubic structure. The XRD peak of BTMO/rGO nanocomposite is comparatively broader than the BTMO nanocomposite and bare nanoparticles due to the presence of high surface area rGO. From the SEM image it is observed that the BTMO nanocomposite has comparatively larger particles than the bare nanoparticles and BTMO/rGO nanocomposites. Hence, the BTMO/rGO nanocomposite has alteration in surface to volume ratio and improved electron conductivity were observed with increased integral area and current such as 2.5117×10^{-4} A/s and 3.1686×10^{-4} A respectively in CV behavior, when it is compared to BTMO nanocomposite and bare nanoparticles. The BTMO/rGO nanocomposite also has an increased specific capacitance value of 317.2 F/g at 1 A/g. The increased specific capacitance value of BTMO/rGO nanocomposites are mainly due to the synergistic effect between $\text{SnO}_2/\text{Co}_3\text{O}_4$ and rGO. Hence, it may be responsible for the improved electron conductivity, due to the free diffusion pathway for the fast ion movement and also it has easily ion accessibility nature to the storage sites makes the materials with both the electric double layer capacitance and pseudocapacitance behavior. Hence, BTMO/rGO nanocomposite would be a promising candidate material for energy storage supercapacitor application.

1 Introduction

Nanomaterials are in need for the betterment of energy storage devices and supercapacitors. Due to the advancement in nanomaterials research nowadays, there are many permutable combinations of new nanomaterials are identified with

longer cycle life (> 100,000 cycles), high power density etc., when it is compared to conventional dielectric capacitors. Those nanomaterials show an excellent energy density, rapid charge/discharge rate and low maintenance cost etc., [1]. Based on the energy storage mechanism, the supercapacitors are classified as electric double layer capacitors (EDLC) and fast reversible faradic pseudocapacitors [2].

Recently, metal oxide nanoparticles such as SnO_2 , ZnO, TiO_2 and WO_3 have attracted extensive research interests owing to their unique physical and chemical properties and diverse potential applications in optical and electronic fields based research shows dramatic improvement in the field of supercapacitors applications [3, 4]. Among various metal oxide nanoparticles, SnO_2 gains importance because of its n-type semiconductor property with a wide band gap of ($E_g = 3.6$ eV at 300 K), high chemical stability, temperature stability, excellent electron conductivity, optical property, mechanical property and electrochemical properties etc., [5–7]. The redox activity of SnO_2 nanomaterials, it is widely considered as an anode material in lithium ion batteries [8, 9]. The SnO_2 nanoparticles has shorter electron transporting

Electronic supplementary material The online version of this article (<https://doi.org/10.1007/s10854-018-9272-0>) contains supplementary material, which is available to authorized users.

✉ G. Sasikala
sasikalaganapathycgc@gmail.com;
sasikala_ganapathy@yahoo.co.in

¹ Crystal Growth Centre, Anna University, Chennai 600 025, India

² Research and Development, Dhanalakshmi College of Engineering, Manimangalam, Tambaram, Chennai 601 301, India

³ Department of Medical Physics, Anna University, Chennai 600 025, India

paths and also it has high surface-to-volume ratio, hence the bare nanoparticles has poor electrical conductivity. To improve the electrical conductivity of the material, the bare nanoparticle SnO₂ combined with activated carbon or graphene, a conductive materials is another very promising material to improve electronic conductivity and accommodate volume change of metal oxide active materials during cycling [10]. However, SnO₂ has both the charge/discharge property, superior chemical stability and excellent electrical conductivity, when it combines to graphene, which makes the composite material with both buffer accommodate volume change and also it improves the electrical conductivity of the material. It is mainly due to the change in surface to volume ratio of the SnO₂/rGO nanocomposite when compared to bare nanoparticles [11, 12]. SnF₂/C composite materials were also widely considered as an anode material due to its improved discharge and charge capacities. SnF₂/C composite material showed superior cycling stability when compared to bare nanoparticle such as SnF₂ composites [13].

In recent years, many researchers reported that the transition metal oxides such as MnO₂ [14], Co₃O₄ [15], Fe₂O₃ [16] and NiO₂ [17] are also widely considered because of it energy storage properties (the d-shell elements usually has higher free electron carrying property) [18]. Among various transition metal oxides, Co₃O₄ is widely considered for its unique energy storage, catalytic activity, magnetic behavior, adsorption properties and eco-friendliness etc., [19–21]. However, the Co₃O₄ nanoparticles has high electron storage property but the bare nanoparticle has poor electron conductivity. It is so because of its larger crystalline size, the bare Co₃O₄ nanoparticle has poor capability and reversibility in charge/discharge rate of the materials. Even though, the p-type semiconductor Co₃O₄ nanomaterials possesses poor electronic conductivity, when it combined with high conducting materials such as carbon black shows the improved electron conductivity than the Co₃O₄ bare nanoparticles [22]. Due to the reduced particle size and improved surface area of the nanocomposites, when it is compared to the bare nanoparticles shows better charge–discharge activity and improved energy storage property of the materials. Hence, transition metal oxide Co₃O₄-rGO nanocomposites are widely considered has a candidate for the supercapacitor application [22–24].

Different combinations of metal oxide and transition metal oxide nanocomposites are commonly known as binary transition metal oxide (BTMO) are widely considered because of it's unique physical, chemical, electrical, optical and magnetic properties. Researchers in the field of basic research gives much more attention to BTMO nanocomposite materials and make them in use for technological applications such as energy storage devices in particular for supercapacitor etc. Nowadays, there are many different combinations of metal oxides and transition metal oxide

nanocomposites alone and in combination with rGO such as Co₂SnO₄/activated carbon composite electrode for super capacitor applications [25], SnO₂ coated Co₃O₄ hollow nano spheres used in Li-ion batteries shows extraordinary performance [26] etc.,

In recent year carbonaceous materials such as MWCNTs, reduced graphene oxide, acetylene black etc, plays an important role in electrochemical energy storage devices, due to their high mechanical, thermal stability and excellent electrical conductivity [13, 27, 28]. Carbon based materials such as graphene are widely considered as an electronic material. Graphene is a two-dimensional single atom thick membrane of carbon atoms arranged in a honeycomb crystal [29] and also it has mechanically strong, transparent, thin flexible conductor and excellent electrical conductivity [30].

In this regard, a pilot attempt were made to synthesized and characterize the SnO₂-Co₃O₄/rGO (BTMO/rGO) nanocomposites by co-precipitation method and the same were compared to SnO₂, Co₃O₄ bare nanoparticles and BTMO nanocomposites. The structural morphology and crystallinity of the synthesized nanomaterials were determined by X-ray diffraction (XRD), surface morphology by scanning electron microscopy (SEM), the functional groups by Fourier transform infrared (FT-IR) and Raman spectroscopic studies. Electrochemical properties of the synthesized materials were also determined by recording cycling voltammogram (CV), galvanostatic charge–discharge and electrochemical impedance spectroscopy (EIS). From the charging and discharging spectra, the specific capacitance value of the nanomaterials were calculated. From the CV result, cyclic behavior of bare nanomaterials such as SnO₂, Co₃O₄, BTMO nanocomposites and BTMO/rGO composites were compared and discussed.

2 Experimental

2.1 Materials

Tin(II)chloride (SnCl₂) molecular weight (MW) 189.62 g/mol, product no. 208256, 98% pure reagent grade chemical were purchased from Sigma Aldrich, Saint Louis, MO 63103, USA. Cobalt(II)chloride (CoCl₂) MW 129.84 g/mol, product no. 60,818, 98% pure reagent grade chemical were purchased from Sigma Aldrich Pvt. Ltd, Bangalore, INDIA. Graphene oxide powder MW 4239.48 g/mol, product no. 796034, powder of 15–20 sheets, 4–10% edge oxidized were purchased from Sigma Aldrich, Saint Louis, MO 63103, USA. Sodium hydroxide (NaOH) MW—40 g/mol, product no. S8045, 98% pure pellets were purchased from Sigma Aldrich, Saint Louis, MO 63103, USA were utilized for the experiment.

2.2 Synthesis of SnO₂ nanoparticle

2.2563 g of SnCl₂ was dissolved in 100 ml of distilled water. The above solution were stirred well for 5 h at 60 °C. The final pH of the solution were adjusted to pH-7 using 0.1 mol (M) of NaOH solution, at pH-7 a white precipitate appears and the obtained precipitate were filtered using wattman grade-1 (4 mm) filter paper and the same were washed for 4–5 times with ethanol and distilled water.

2.3 Synthesis of Co₃O₄ nanoparticle

2.379 g of cobalt chloride were dissolved in 100 ml of distilled water. The resultant solution were stirred well for 5 h at 60 °C. Then the pH of the above solution adjusted to pH-7 using 0.1 M of NaOH solution, at pH-7 a brown precipitate appears and the resultant brown precipitate were collected by filtration using wattman grade-1 (4 mm) filter paper, and then the filtrate were washed 4–5 times using ethanol and distilled water.

2.4 Synthesis of BTMO nanocomposite

The BTMO nanocomposite materials were synthesized by co-precipitation method. First, 1.579 g of SnCl₂ were added to 100 ml distilled water taken in a beaker, then 0.713 g of CoCl₂ were also added pinch by pinch into it. The above solution were stirred vigorously 5 h at 60 °C. Finally, the pH of the above solution were adjusted to 7 using 0.1 M of NaOH solution. When the reaction mixture reaches to pH-7, a brown precipitate appears. The resultant precipitate were collected by filtration using watt man grade-1 (4 mm) filter paper, then the filtrate was washed for 4–5 times using ethanol and distilled water.

2.5 Synthesis of BTMO/rGO nanocomposite

The BTMO/rGO nanocomposite materials were also synthesized by co-precipitation method. Here first, 0.1 g of graphene oxide were dissolved in 100 ml distilled water, then the solutions were kept under sonication for 1 h. After 1 h, 1.579 g of SnCl₂ and 0.713 g of Co₃O₄ were added into the solution, then the reaction mixture were stirred well for 5 h at 60 °C. The pH of the solution were adjusted to 7 using 0.1 M NaOH solution. When the pH of the solution reaches to 7, a black color precipitate appears. The above precipitate were collected by filtration using watt man grade-1 (4 mm) filter paper, and then the filtrate were washed 4–5 times using ethanol and distilled water. After final washing, all the resultant precipitates were allowed to

dry at 60 °C in vacuum oven for 24 h, then the composite were annealed at 300 °C for 5 h.

2.6 Characterization equipment

The synthesized bare nanoparticles, BTMO and BTMO/rGO nanocomposites purity and lattice parameters were determined by recording the XRD pattern using PAN analytical X-ray diffraction instrument. The crystalline nature of the prepared nanomaterials were analyzed with the source wavelength of 1.542 Å Cu K α radiation. The surface morphology and microstructure of the synthesized nanomaterials were determined using Carl Zeiss instruments model no. MA15/EVO-18, with electron high tension of 10.00 kV with the wide angle of 10.5 mm along with the magnification range starts from $\times 20,000$ ($\times 20.00k$). The functional group rotational vibration of the synthesized materials were determined by recording FT-IR spectra with the spectral range from 400 to 4000 cm⁻¹ using Frontier Biodiesel FAME Analyzer, model no. L125000P from Perkin Elmer instruments, USA. The Micro Raman spectrometer from Renishaw instrument, model RM¹⁰⁰⁰ were used to study the functional group excitation vibration of the synthesized nanomaterials using 532 nm Nd–YAG laser as an excitation source. The Cyclic Voltammetry instruments from Sinsil International, Ahmedabad, Gujarat, India. were utilized to calculate the electrochemical properties of the synthesized nanomaterials.

2.7 Preparation of modified glassy carbon electrode

The modified glassy carbon electrode (GCE) were prepared by mixing the synthesized nanomaterials with the carbon black and polyvinylidene fluoride (PVDF) in weight percentage of 80:10:10 respectively. The mixture were dispersed in 20 μ l of 80% ethanol and 20 μ l of dimethylformamide (DMF), the same were sonicated for 1 h. Then the suspension were dropped onto the GCE and dried at 80 °C for 5 h. The electrochemical properties of the modified electrode were investigated under a standard three-electrode cell, which also includes platinum electrode (counter) and Ag/AgCl (reference electrode) respectively. The CV, galvanostatic charge/discharge and electrochemical impedance spectroscopy (EIS) were performed on an electrochemical workstation (Auto lab PGSTAT302, Metrohm). The CV measurements were carried out in a potential range of –0.2–0.7 V at different scan rates. Galvanostatic charge/discharge curves were measured in the same potential range at different current densities. Electrochemical Impedance Spectroscopy (EIS) measurements were recorded in the frequency range from 1 Hz to 100,000 kHz at 5 mV amplitude which was referring in to the open circuit potential.

3 Result and discussion

3.1 XRD measurements

The XRD patterns of synthesized nanomaterials were shown in Fig. 1. Figure 1a represents the XRD pattern of SnO₂ nanoparticles with the corresponding 2θ peak value of 26.6°, 33.9°, 38°, 42.5°, 51.9°, 54.5°, 58.2°, 62.05°, 64.8°, 66.0°, 71.1° and 78.7° which is associated to (110), (101), (200), (210), (211), (220), (002), (310), (112), (301), (202) and (321) planes respectively. The obtained XRD pattern the synthesized materials are matched to the standard (hkl) planes of SnO₂ and hence, the obtained result represents that the synthesized materials is in the form of SnO₂ having a tetragonal rutile structure, which are in good agreement with the literature values of JCPDS card no. 41-1445 [3, 31]. Figure 1b represents the Co₃O₄ nanoparticle with the corresponding 2θ peak values at 19.072°, 31.2°, 36.82°, 38.5°, 55.64°, 59.12° and 65.15° which indicate the plane (111), (220), (311), (222), (440), (422), (511) and (440) respectively. The obtained XRD pattern the synthesized materials are in good agreement to the standard (h k l) planes of Co₃O₄

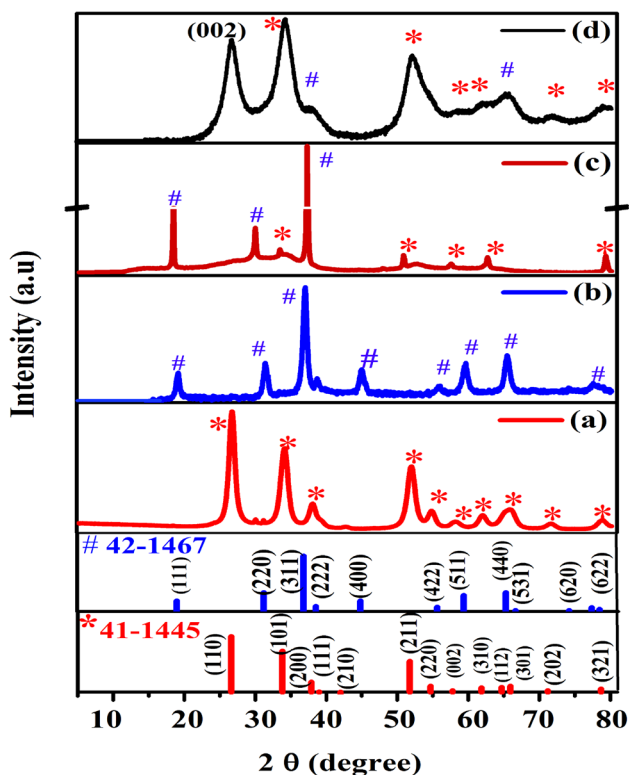


Fig. 1 XRD Pattern of synthesized nanomaterials along with JCPDS card no. 41-1445 represents SnO₂ and JCPDS card no. 42-1467 represents Co₃O₄ for better understanding. 1 (a) the XRD pattern of synthesized SnO₂ nanoparticles, (b) Co₃O₄ nanoparticles, (c) BTMO nanocomposite and (d) BTMO/rGO nanocomposite

JCPDS card no. 42-1467 hence, the obtained result represents that the synthesized material is in the form of spinal cubic structure of Co₃O₄ nanoparticles [20].

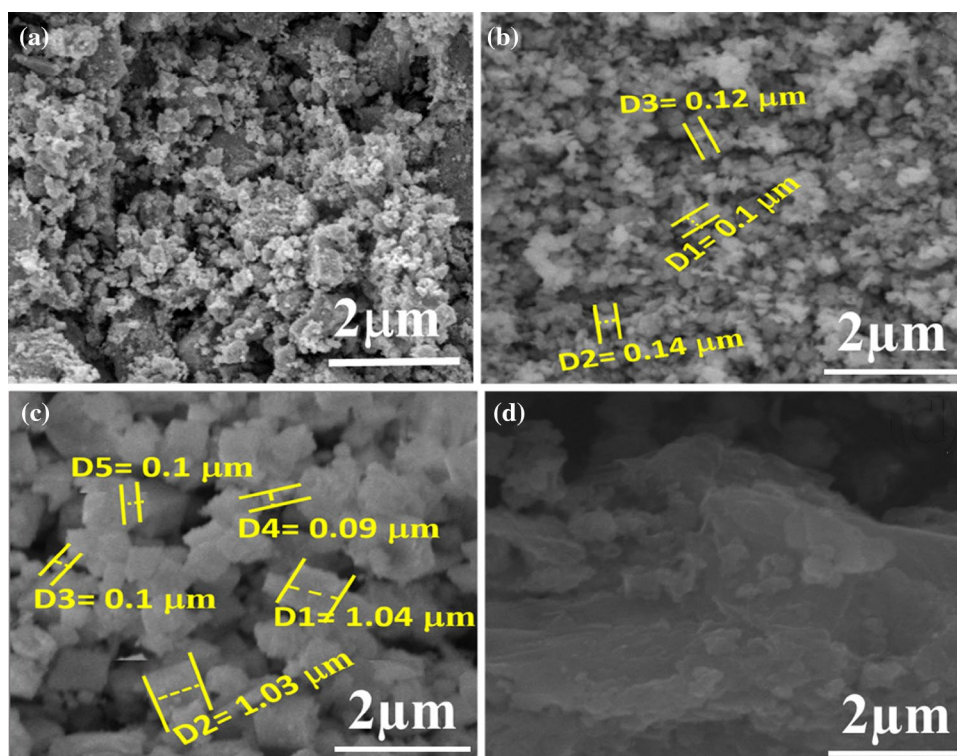
Figure 1c represents the BTMO nanocomposite materials with peaks values of 18.9°, 29.8°, 33.3°, 37.05°, 50.66°, 57.4°, 62.5° and 79.1° with the corresponding plane (111), (220), (101), (311), (211) (002), (221) and (321) respectively were observed. The plane around (111), (220) and (311) corresponds to the spinal cubic structure of Co₃O₄, the plane around (101), (211) (002), (221) and (321) associated to the tetragonal structure of SnO₂. Based on the obtained result, it is concluded that the synthesized BTMO composite material has both the SnO₂ and Co₃O₄ materials may fused together and form the BTMO nanocomposites. The peak intensity of Co₃O₄ are comparatively higher and sharper than the bare nanoparticles, which may be due to larger cubic crystalline nature of Co₃O₄, it is so because of the Co₃O₄ has comparatively larger ionic radius than SnO₂ in this nanocomposite [32]. Hence, BTMO nanocomposites may have with improved crystalline Co₃O₄ along with the fine crystalline SnO₂ in the nanocomposites were determined.

Figure 1d represents the XRD pattern of BTMO/rGO nanocomposites, the peaks observed around 26.4°, 33.88°, 37.52°, 51.94°, 65.14° and 71.5° with the corresponding plane (002), (110), (101), (311), (211), (440) and (320) respectively. Here, the plane around (002) may be corresponds to the presence of rGO, the plane around (110), (101), (211) and (320) represents the presence of SnO₂, and the plane around (311) and (440) represents the presence of Co₃O₄. Based on the obtained results it is observed that the peaks are broader than the bare nanoparticles and BTMO nanocomposite. It may be due to the presence higher surface area carbon atom along with the composite materials. The higher surface area carbon atom may also influence further reduction of particles size of nanomaterials such as SnO₂ and Co₃O₄ in the nanocomposite [22]. Hence, the particle size SnO₂ nanoparticles reduced further when compared to bare nanoparticle (SnO₂) and also the particle size. The surface area of SnO₂ are comparatively higher than the Co₃O₄. In this regard, the peaks of SnO₂ dominates over Co₃O₄ in the BTMO/rGO nanocomposite.

3.2 SEM with EDAX

The surface morphology and microstructure of the synthesized nanomaterials were determined by recording SEM image and the same were shown in Fig. 2. Figure 2a represents the SEM image of SnO₂ nanoparticles. From the figure, it is observed that the synthesized nanoparticles has fine crystalline nature. The respective EDAX pattern of SnO₂ bare nanoparticles were shown in Fig. s1a, from the Fig. s1a it is confirmed that the synthesized material

Fig. 2 SEM image of **a** SnO₂ nanoparticles, **b** Co₃O₄ nanoparticles, **c** BTMO nanocomposite and **d** BTMO/rGO nanocomposite



has Sn and O elemental peaks only. Figure 2b represents the SEM image of Co₃O₄ nanoparticles. From the figure, it is observed that the synthesized nanoparticles has fine cubic shape crystals with averaged particles size of around 0.1 μm. The respective EDAX pattern of Co₃O₄ were shown in Fig. s1b. From the Fig. s1b it is confirmed that the synthesized material has Co and O elemental peaks. Figure 2c represents the SEM image of BTMO nanocomposite. From the figure, it is observed that the synthesized nanocomposite has comparatively larger cubic crystals with average particle size of around 1.04 μm, along with fine rutile crystals of SnO₂ nanoparticles were also present in it. The respective EDAX pattern of BTMO nanocomposite were shown in Fig. s1c. From the Fig. s1c it is confirmed that the synthesized material has Sn, O and Co element peaks alone. The SEM and it EDAX pattern has in good agreement to the XRD result. Figure 2d represents the SEM image of synthesized BTMO/rGo nanocomposite material. From the figure, it is observed that the SnO₂ and Co₃O₄ uniformly merged onto the surface of reduced graphene oxide sheet. The EDAX pattern of BTMO/rGO nanocomposite materials were shown in Fig. s1d, from the figure it is confirmed that the synthesized materials shows predominant peaks of C, Sn, O and Co elemental peaks only. The respective EDAX spectra confirms the presence of carbon element along with the BTMO nanocomposites

and the obtained results are in good agreement to the XRD.

3.3 FT-IR spectroscopy

The synthesized SnO₂ and Co₃O₄ bare nanoparticles, BTMO and BTMO/rGO nanocomposite materials were subjected to confirm the functional group rotational vibration by recording FT-IR spectra with the spectral range from 40 to 4000 cm⁻¹ and the same were shown in Fig. 3. Figure 3a represents the FTIR spectra of the SnO₂ bare nanoparticles. The dip in the spectra around 3438–3900 and 1629 cm⁻¹ were due to stretching vibration of water molecules. The band at 2290 cm⁻¹ assigned to C–H stretching and bending vibration. The vibration around 667 cm⁻¹ is assigned to anti-symmetric Sn–O–Sn stretching mode of the surface bridging oxides formed by condensation of adjacent surface hydroxyl group vibration. The obtained results confirm the SnO₂ nanoparticle formation [5]. Figure 3b represents the FT-IR spectra of the Co₃O₄ nanoparticles, the following dips were observed around 3447, 2371, 1647, 663 and 570 cm⁻¹. The band at 570 cm⁻¹ was assigned to Co–O stretching vibration mode and 663 cm⁻¹ assigned to the bridging vibration of O–Co–O band. The weak band near 1647 and 3447 cm⁻¹ is assigned to H–O–H bending vibration mode were presented due to the moisture [19, 20]. Figure 3c represents the BTMO nanocomposite functional group vibrations; the

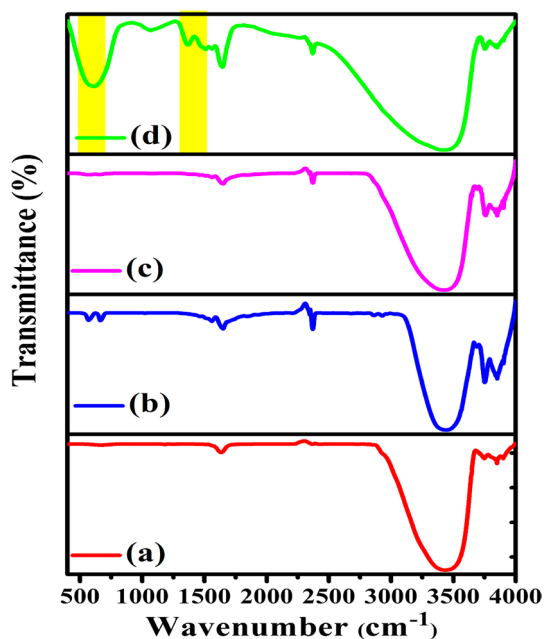


Fig. 3 FR-IR vibration spectra of synthesized nanomaterials, 3 (a) the FT-IR functional group vibrations of synthesized SnO₂ nanoparticles, (b) Co₃O₄ nanoparticles, (c) BTMO nanocomposite and (d) BTMO/rGO nanocomposite

following dips were observed around 570, 1653, 2372, 3422 and 3853 cm⁻¹. The small dip 570 cm⁻¹ confirm the Sn–O stretching vibration, 3422–3853 and 1653 cm⁻¹ were due to stretching vibration of water molecules. Figure 3d represents the BTMO/rGO nanocomposites functional groups vibrations. The dip at 570, 1653, 2372, 3422 and 3853 cm⁻¹ confirms BTMO nanocomposite form along with the above an another dip around 1465 cm⁻¹ belongs to the vibrations of rGO present in the nanocomposites. The FT-IR functional group vibration spectra are in good agreement to the XRD and SEM with EDAX results.

3.4 Raman spectroscopy

The functional group excitation vibrations of the synthesized nanomaterials were determined by recording Raman spectra and the same were represented in Fig. 4. Figure 4a represents the Raman vibration spectra of SnO₂ nanoparticles. The peaks observed at around 632 and 773 cm⁻¹ result from the rutile SnO₂ nanoparticles, which may assigned to the A_{1g}, B_{2g} vibration mode of SnO₂ nanoparticles respectively [33]. Figure 4b represents the vibration spectra of Co₃O₄ the peaks observed at around 185, 471, 510 and 655 cm⁻¹ may assigned to F_{2g}, E_g, F_{2g} and A_{1g} modes of Co₃O₄ [34, 35]. Figure 4c represents the vibration spectra of SnO₂/Co₃O₄ nanocomposite were observed around 207, 311, 513, 658 and 747 cm⁻¹ it conform the nanocomposite formations. The excitation level vibration spectra peak around 207,

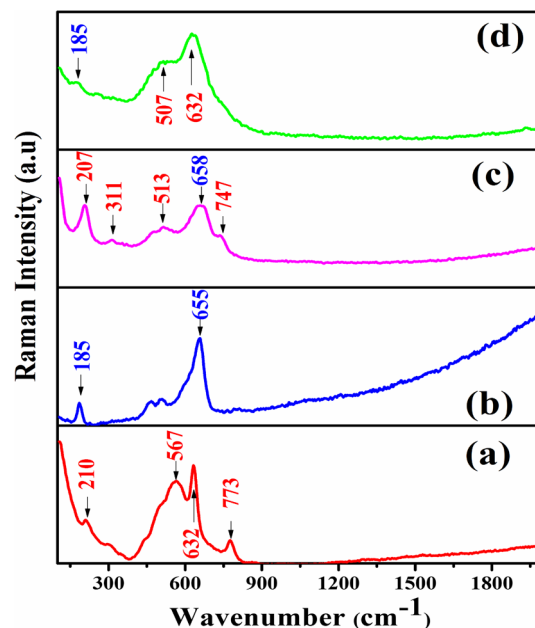


Fig. 4 Raman Spectra of synthesized nanomaterials, 4 (a) represents the functional group Raman vibrations of synthesized SnO₂ nanoparticles, (b) Co₃O₄ nanoparticles, (c) BTMO nanocomposite and (d) BTMO/rGO nanocomposite

311, 513 and 747 cm⁻¹ are may be due to the vibrations of SnO₂ nanoparticles and the strong vibration at around 658 cm⁻¹ are may be due to the presence of Co₃O₄ nanoparticles. Figure 4d represents the vibration spectra of BTMO/rGO composite the peaks observed around 185, 258, 507 and 632 cm⁻¹. The vibration peak around 185 cm⁻¹ may be due to Co₃O₄ nanoparticles, the other vibration peaks around 258, 507 and 632 cm⁻¹ may be due to the presence of SnO₂ nanoparticles, the carbon peak was not observed in the obtained Ramen spectra. It may be due to lesser concentration of carbon or over deposition of SnO₂ and Co₃O₄ nanoparticles on the surface of rGO sheets. In this regards, the Raman vibration peak of carbon are not observed in the BTMO/rGO nanocomposites.

3.5 Electrochemical analysis

3.5.1 Cyclic voltammetric studies

The electrochemical properties of the synthesized bare nanoparticles such as SnO₂ and Co₃O₄, BTMO nanocomposites and BTMO/rGO nanocomposites were investigated by means of cyclic voltammetry (CV) with potential window –0.2 to 0.7 in 1 M H₂SO₄ electrolyte solution. The CV curve of all the synthesized nanomaterials with different scan rate such as 100, 75, 50, 25, 5 mV/s were shown Fig. 5a–d. From the Fig. 5a, b, it is observed that both the synthesised bare nanoparticles such as SnO₂ and Co₃O₄ nanoparticles CV

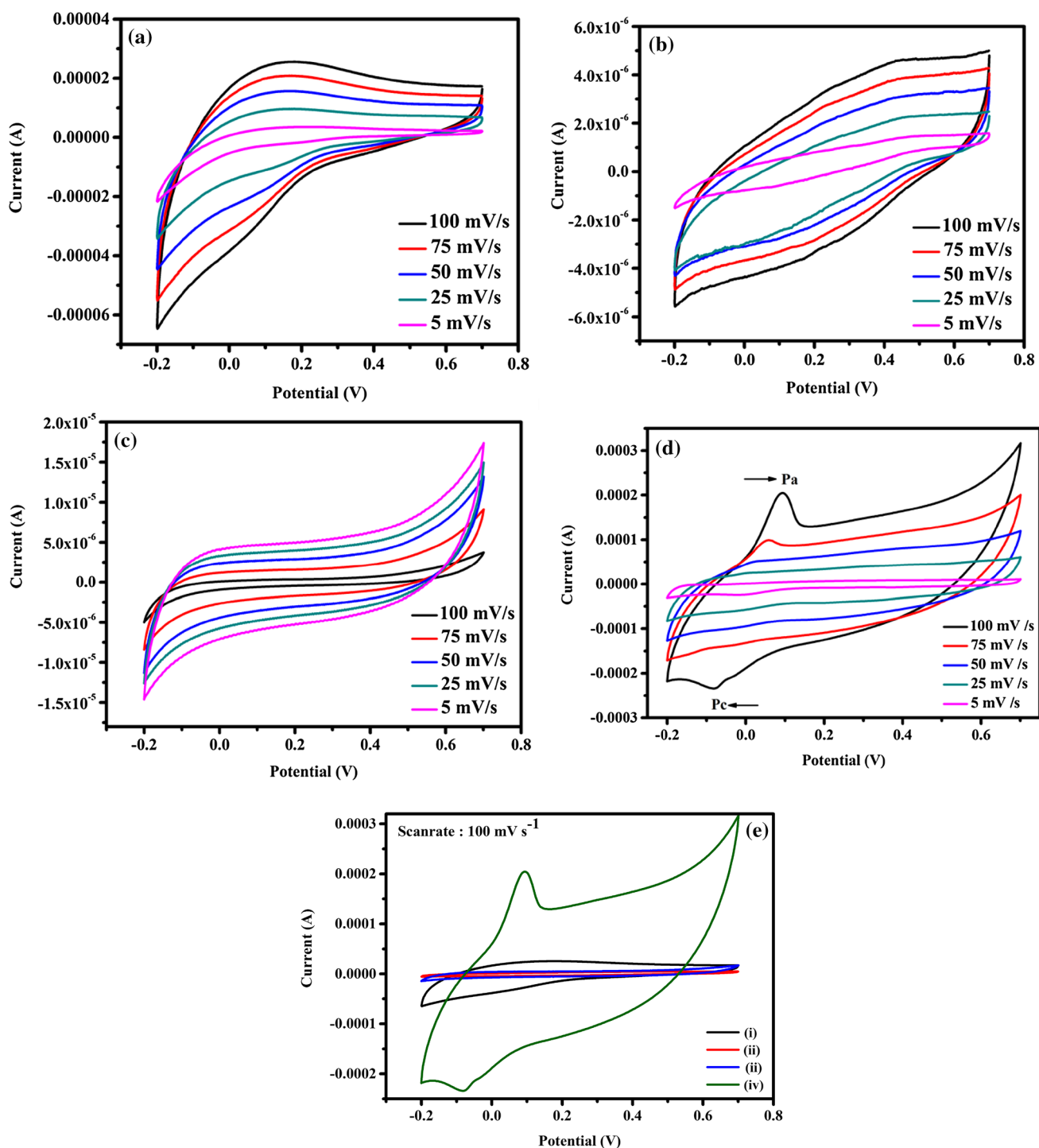


Fig. 5 The cyclic voltammetry of the synthesized **a** SnO₂ nanoparticles, **b** Co₃O₄ nanoparticles, **c** BTMO nanocomposite and **d** BTMO/rGO nanocomposite materials with potential window -0.2 to 0.7 in 1 M H₂SO₄ electrolyte solution with different scan rates of 100 , 75 ,

50 , 25 , 5 mV/s. **e** Represents the comparison of CV curve of SnO₂, Co₃O₄ bare nanoparticles, BTMO nanocomposites and BTMO/rGO nanocomposite with a scan rate of 100 mV/s between -0.2 and 0.7 in 1 M H₂SO₄ electrolyte solution

curve nature and behavior, both the nanoparticles behaves like pseudocapacitance due to their electrochemical properties, with lesser redox peak were observed and the obtained results are well correlated to the previous literature [21, 36].

Figure 5c represents the CV curve and behavior of BTMO nanocomposite materials. During the oxidation/reduction process, the BTMO exhibits smaller and rectangular shaped CV curve, which is due to the typical electric double

layer capacitive behavior and also the reaction mechanism is surface reaction but not diffusion limited at the BTMO composite [28]. The size of the CV loop area of BTMO nanocomposite was less when compared to SnO₂ and Co₃O₄ nanoparticles. Which is mainly due to larger particle size of BTMO nanocomposite with lesser surface to volume ratio. The electrical conductivity of the BTMO was comparatively low because of the larger particle size when it is compared to the bare nanoparticles.

Figure 5d represents CV curve nature and behavior of BTMO/rGO nanocomposite. The BTMO/rGO nanocomposite materials has rectangular shape curve and also it has a pair of well-resolved redox peak with the potential redox value of Pa = 0.0917 V, Pc = -0.0814 V respectively at the scan rate of 100 mV/s. Hence, the BTMO/rGO nanocomposite has combined contribution of both electric double layer capacitance and pseudocapacitance behavior. It may be attributed to the presence of layered morphology of rGO, that reduces the particle size of the SnO₂/Co₃O₄ when the composite have been made with rGO, nanomaterials when compared to bare nanoparticles and BTMO nanocomposite materials. In this regards, the conductivity, chemical stability and mechanical support of the material were increased. Hence, BTMO/rGO nanocomposite shows the hybrid capacitance behavior.

Figure 5e represents the comparison of CV curve of SnO₂, Co₃O₄ bare nanoparticles, BTMO nanocomposites and BTMO/rGO nanocomposite with a scan rate of 100 mV/s between the potential window -0.2 to 0.7 in 1 M H₂SO₄ electrolyte solution. The SnO₂, Co₃O₄ bare nanoparticles shows the nonrectangular behavior due to the faradic redox reaction occurring at CV curve and the result for pseudo capacitance performance. The BTMO nanocomposite shows the rectangular behavior, but the redox peak is absent in the composite and obtained result shows an ideal capacitance behavior. Among the CV curve, the integral area and current of BTMO/rGO composites is larger, which means that this composite has the higher capacitance when compared with bare SnO₂, Co₃O₄ nanoparticles and BTMO nanocomposites and the same were shown in Table 1. The capacitance value of BTMO/rGO composites were enhanced due to synergistic effect between SnO₂/Co₃O₄ and rGO these three material

responsible for the improved electrical conductivity, provides the free diffusion pathway for the fast ion movement and also it has easily ion accessibility nature to the storage sites makes the materials with both supercapacitance and pseudocapacitance behavior.

Figure 6a–d represents the galvanostatic charge/discharge curve of SnO₂, Co₃O₄ bare nanoparticles, BTMO nanocomposite and BTMO/rGO nanocomposite materials were investigated by chronopotentiometry. Form chronopotentiometry the potential window were set between -0.2 and 0.7 at the different current density of 1, 2, 3, 4 and 5 A/g in 1 M H₂SO₄ electrolyte solution. The specific capacitance value calculated from charge discharge curve by using Eq. (1).

$$C = I \times t_d / m \times \Delta V \quad (1)$$

where (I) denotes for the applied current, (t_d) discharge time, (m) mass of active electrode, (ΔV) potential window. The charge/discharge curve of SnO₂, Co₃O₄ bare nanoparticles seems to be an anti-symmetric capacitance behavior and the same were show in Fig. 6a, b. The specific capacitance value for the bare nanoparticles SnO₂ has 122.8, 47.7, 25.3, 20.8 and 19.4 F/g, and Co₃O₄ has 265.7, 124.1, 54.3, 41.3 and 36.6 F/g at the current density of 1, 2, 3, 4 and 5 A/g respectively. Figure 6c represents the specific capacitance behavior of larger crystalline BTMO nanocomposites ranges from 6.1, 3.7, 2.7, 2.1 and 1.1 F/g at the current density 1, 2, 3, 4 and 5 A/g respectively. The specific capacitance values of BTMO nanocomposites has comparatively lesser than the bare nanoparticles. It was so because, the BTMO nanocomposite are comparatively larger crystalline size than SnO₂, Co₃O₄ bare nanoparticles. The larger particle size of Co₃O₄ the materials has lesser electrical conductivity. In this regard, the specific capacitance value of the BTMO nanocomposite material has drastically reduced. Figure 6d represents the charge/discharge pattern of BTMO/rGO nanocomposites materials. The BTMO/rGO nanocomposite has good capacitance behavior when compared to bare nanoparticles and BTMO nanocomposites. The BTMO/rGO nanocomposite has specific capacitance values ranges from 317.2, 316.4, 292.3, 272.4 and 104 F/g, with the current density 1, 2, 3, 4 and 5 A/g respectively.

Figure 6e represents the comparison of galvanostatic the charge/discharge behavior of (i) SnO₂ nanoparticles, (ii) Co₃O₄ nanoparticles, (iii) BTMO nanocomposite and (iv) BTMO/rGO nanocomposites were investigated by chronopotentiometry with the potential range between -0.2 and 0.7 at a current density 1 A/g in 1 M H₂SO₄ electrolyte solution. The charge/discharge behavior of BTMO/rGO nanocomposites has longer time duration when compared to SnO₂, Co₃O₄ nanoparticles and BTMO nanocomposites, which indicating higher specific capacitance nature of BTMO/rGO nanocomposites based supercapacitance. The specific capacitance values for SnO₂, Co₃O₄, BTMO composites and BTMO/rGO

Table 1 CV curve integral area and current of SnO₂, Co₃O₄, BTMO and BTMO/rGO nanocomposite for the scan rate of 100 mV s⁻¹

S. no.	Materials	Integral area (A/s)	Current (A)
1	SnO ₂	3.5557 × 10 ⁻⁵	2.557 × 10 ⁻⁵
2	Co ₃ O ₄	5.3294 × 10 ⁻⁶	5.579 × 10 ⁻⁶
3	SnO ₂ /Co ₃ O ₄ (BTMO)	1.0924 × 10 ⁻⁵	3.5557 × 10 ⁻⁵
4	BTMO/rGO nanocomposite	2.5117 × 10 ⁻⁴	3.1686 × 10 ⁻⁴

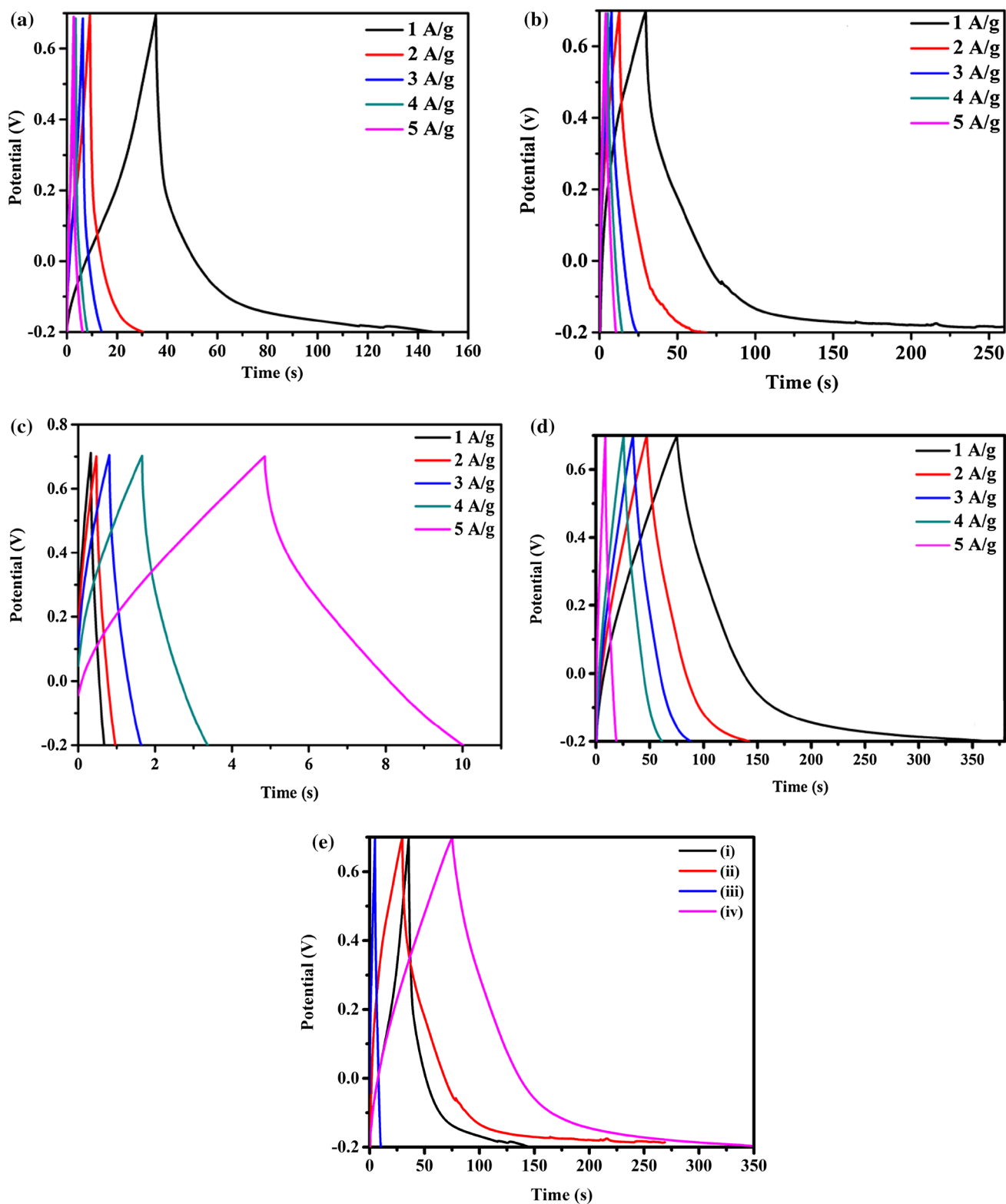


Fig. 6 Represents the galvanostatic charge/discharge curve of **a** SnO₂ nanoparticles, **b** Co₃O₄ nanoparticles, **c** BTMO nanocomposites and **d** BTMO/rGO nanocomposites were investigated by chronopotentiometry with the potential range between -0.2 and 0.7 at a current density 1, 2, 3, 4, 5 A/g in 1 M H₂SO₄ electrolyte solution. **e** repre-

sents the comparison of galvanostatic the charge/discharge behavior of (i) SnO₂ nanoparticles, (ii) Co₃O₄ nanoparticles, (iii) BTMO nanocomposites and (iv) BTMO/rGO nanocomposites were investigated by chronopotentiometry with the potential range between -0.2 and 0.7 at a current density 1 A/g in 1 M H₂SO₄ electrolyte solution

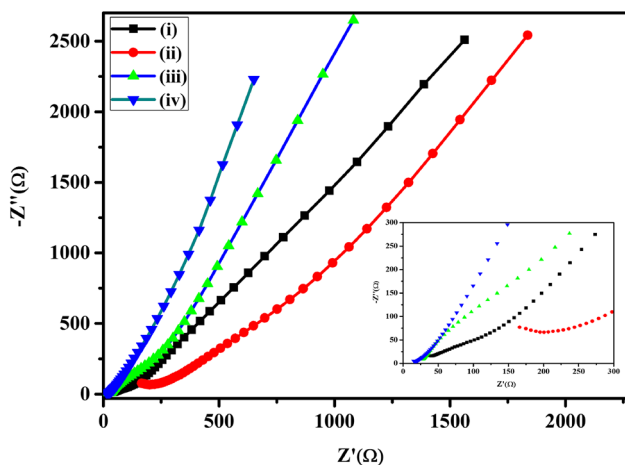


Fig. 7 Represents the Nyquist plots of the EIS are tested in the frequency range from 1 to 1,00,000 Hz at open circuit potential with amplitude of 5 mV for (i) SnO₂, (ii) Co₃O₄ bare nanoparticles, (iii) BTMO nanocomposites and (iv) BTMO/rGO nanocomposite. The inset represents the zoomed semicircle view

nanocomposites charge/discharge curves values ranges from 122.8, 265.7, 6.1 and 317.6 F/g respectively. The enhancement in the specific capacitance behavior of BTMO/rGO nanocomposites are may be due to the presence of higher surface to volume ratio, electron conductivity, chemical stability, mechanical stability and improved storage capacity.

The kinetic and mechanistic information of prepared electrode materials can be evaluated by electrochemical impedance spectroscopy (EIS). The EIS are tested in the frequency range from 1 to 1,00,000 Hz at open circuit potential with amplitude of 5 mV, where Z' and Z'' are the real and imaginary parts of the impedance respectively. Figure 7 shows the Nyquist diagrams of SnO₂, Co₃O₄ bare nanoparticles, BTMO nanocomposites and BTMO/rGO nanocomposite. According to the analysis, the Nyquist diagram of electrodes displays a semicircle in the high frequency region and a linear in the low-frequency region. The diameter of semicircle presents in the high frequency region suggests that there is a charge transfer resistance (R_{ct}) in the electrochemical system, which correlates the diffusion of charge. Obviously, the smaller semicircle in BTMO/rGO means charge transfer resistance (R_{ct}) decreases which may attributed to the synergistic effect between the BTMO when it combined to rGO, which may be responsible for improved electrical conductivity when compared to SnO₂, Co₃O₄ and BTMO composites. This result indicates that the composite providing an ideal pathway for easy and fast penetration of the electrolyte ions into the inner layer of the BTMO/rGO composites. The vertical line at lower frequencies indicates an ideal capacitive behaviour, representative of the ion diffusion of electrolyte within the pores of the electrode.

4 Conclusion

Based on the obtained results, it is concluded that the synthesized BTMO/rGO nanocomposites has improved integral area and increased current such as 2.5117×10^{-4} A/s and 3.1686×10^{-4} A respectively in CV behavior, when it is compared to BTMO nanocomposite and bare nanoparticles. The BTMO/rGO nanocomposite also has an increased specific capacitance value of 317.2 F/g at 1 A/g. This may be due to the synergistic effect between BTMO and rGO. It may be responsible for the improved electron conductivity due to free diffusion pathways and the fast ion movement in BTMO/rGO nanocomposites when compared to the BTMO nanocomposite and bare nanoparticles. It may be due to the presence of high electron conducting reduced graphene oxide present along with the BTMO nanocomposite. Hence, the BTMO/rGO nanocomposite materials show both EDLC and pseudocapacitance behavior. In this regards the BTMO/rGO nanocomposite material may be considered for the betterment of supercapacitor applications.

Acknowledgements The author S. Nagarani, acknowledge the research scholars from the Department of Physics, Department of Medical Physics, Department of Chemistry, Centre for Nanoscience and technology of Anna University, Chennai-25 for them kind support. The author whole-heartedly acknowledge the Director of Centre for Research, Professor R. Jayavel for his kind support to extend the lab facility to carry out the research work.

Compliance with ethical standards

Conflict of interest The authors declares that there is no conflict of interest regarding the publication of this paper.

References

- R.B. Rakhi, H.N. Alshareef, *J. Power Sources* **196**, 8858–8865 (2011)
- L.L. Zhang, X.S. Zhao, Carbon-based materials as supercapacitor electrodes. *Chem. Soc. Rev.* **38**, 2520–2531 (2009)
- W. Chen, D. Ghosh, S. Chen, *J. Mater. Sci.* **43**, 5291–5299 (2008)
- Z. Qinqin, M. Lisha, Z. Qiang, W. Chenggang, X. Xijin, *J. Nanomater.* (2015). <https://doi.org/10.1155/2015/850147>
- L. Tan, L. Wang, Y. Wang, *J. Nanomater.* **2011**, 1–10 (2011)
- Q. Gao, H. Jiang, M. Li, P. Lu, X. Lai, X. Li, Y. Liu, C. Song, G. Han, *Ceram. Int.* **40**, 2557–2564 (2014)
- M.K. Roković, G. Ljubek, M. Žic, J. Popović, *Croat. Chem. Acta* **90**(2), 289–295 (2017)
- X. Meng, M. Zhou, X. Li, J. Yao, F. Liu, P. Xiao, Y. Zhang, H. He, *Electrochem. Acta* **109**, 20–26 (2013)
- N. Wan, X. Lu, Y. Wang, *Sci. Rep.* **6**, 18978 (2015)
- B. Zhao, S.Y. Huang, T. Wang, K. Zhang, M.M.F. Yuen, J.B. Xu, X.Z. Fu, R. Sun, C.P. Wong, *J. Power Sources* **298**, 83–91 (2015)
- X. Zhua, Y. Zhub, S. Murali, M.D. Stoller, R.S. Ruoff, *J. Power Sources* **196**, 6473–6477 (2011)

12. S. Ren, Y. Yang, M. Xu, H. Cai, C. Hao, X. Wang, *Colloids Surf. A* **444**, 26–32 (2014)
13. G. Ali, J.H. Lee, S.H. Oh, H.G. Jung, K.Y. Chung, *Nano. Energy* **42**, 106–114 (2017)
14. S.R. Srither, A. Karthik, S. Arunmetha, D. Murugasen, V. Rajendran, *Mater. Chem. Phys.* **183**, 375–382 (2016)
15. Y. Gao, S. Chen, D. Cao, G. Wang, J. Yin, *J. Power Sources* **195**, 1757–1760 (2010)
16. P.M. Kulal, D.P. Dubal, C.D. Lokhande, V.J. Fulari, *J. Alloys Compd.* **509**, 2567–2571 (2011)
17. M.S. Wu, M.J. Wang, *Chem. Commun.* **46**, 6968–6970 (2010)
18. J. Jiang, F. Wei, G. Yu, Y. Sui, *J. Nanomater.* **2015**, 1–6 (2015)
19. M. Kumar, A. Subramani, K. Balakrishnan, *Electrochim. Acta* **149**, 152–158 (2014)
20. D. Zhang, F. Li, A. Chen, Q. Xie, M.Y. Wang, X. Zhang, J. Gong, G. Han, A. Ying, Z. Tong, *Solid State Sci.* **13**, 1221–1225 (2011)
21. S.K. Meher, G.R. Rao, *J. Phys. Chem.* **115**, 15646–15654 (2011)
22. L.J. Xie, J.F. Wu, C.M. Chen, C.M. Zhang, J.L. Wang, Q.Q. Kong, C.X. Lv, K.X. Li, L. Wan, G.H. Sun, *J. Power Sources* **242**, 148–156 (2013)
23. M.J. Deng, F.L. Huang, I.W. Sun, W.T. Tsai, J.K. Chang, *Nanotechnology* **20**, 175602 (2009)
24. D. Ghosh, J. Lim, R. Narayan, O.S. Kim, *Appl. Mater. Interfaces* **8**, 22253–22260 (2016)
25. P. He, Z. Xie, Y. Chen, F. Dong, H. Liu, *Mater. Chem. Phys.* **137**, 576–579 (2012)
26. W.S. Kim, Y. Hwa, H.C. Kim, J.H. Choi, H.J. Sohn, S.H. Hong, *Nano Res.* **7**, 1128–1136 (2014)
27. G. Ali, J.H. Lee, B.W. Cho, K.W. Nam, D.A.W. .Chang, S.H. Oh, K.Y. Chung, *Electrochim. Acta* **191**, 307–316 (2016)
28. G. Ali, A. Mehmood, H.Y. Ha, J. Kim, K.Y. Chung, *Sci. Rep.* **7**, 40910 (2017)
29. A.K. Geim, K.S. Novoselov, *Nat. Mater.* **6**, 183–191 (2007)
30. J. Gao, C. Liu, L. Miao, X. Wang, Y. Chen, *J. Electron. Mater.* **45**, 1290–1295 (2016)
31. M. Aziz, S.S. Abbas, W.R.W. Baharom, W.Z.W. Mahmud, *Mater. Lett.* **74**, 62–64 (2012)
32. B.G.S. Raj, J.J. Wu, A.M. Asiri, S. Anandan, *RSC Adv.* **00**, 1–3 (2013)
33. E. Fazio, F. Neri, S. Savasta, *Phys. Rev. B* **85**, 195423 (2012)
34. M. Rashad, M. Rüsing, G. Berth, K. Lischka, A. Pawlis, *J. Nanomater.* (2013). <https://doi.org/10.1155/2013/714853>
35. I. Lorite, J.J. Romero, J.F. Fernández, *J. Raman Spectrosc.* **43**, 1443–1448 (2012)
36. Z.J. Li, T.X. Chang, G.Q. Yun, Y. Jia, *Power Technol.* **224**, 306–310 (2012)